

# Investigating the nanostructured gold thin films using the multifractal analysis

R. P. Yadav · U. B. Singh · A. K. Mittal · S. Dwivedi

Received: 2 May 2014 / Accepted: 17 July 2014 / Published online: 31 July 2014  
© Springer-Verlag Berlin Heidelberg 2014

**Abstract** The atomic force microscopy images representing the surface morphology of the nanostructured gold thin films of thickness of 20, 50 and 200 nm, respectively, were investigated using the multifractal analysis. The interface width and growth exponent corresponding to films of different thicknesses were estimated. The surfaces having greater roughness give rise to larger nonlinearity and wider width of the multifractal spectrum. The statistical tests confirm that the gold thin film surfaces under investigation are multifractal in nature.

## 1 Introduction

Gold is a dense, soft and ductile metal with bright yellow colour. It is considered attractive due to its lustre and resistance to tarnishing in air or water. It is a transition metal which is solid under standard conditions. It has many practical applications in various fields such as optical [1], electronics [2], electrochemical [3], photoelectrochemical [4], surface-enhanced Raman scattering (SERS) [5], superhydrophobicity [6], catalysis [7], sensors [8] and medicine [9]. The morphology of gold surface, mainly its

roughness, influences the functional properties. It is particularly important for SERS [10, 11] and superhydrophobicity applications [6] because signal enhancement factor and contact angle are directly related to the nano-scale morphology.

The nanostructured thin films play important role in different fields of material science and technology. The thin film growth under nonequilibrium conditions is a complicated stochastic process. The study of growing surface morphologies and their implications for physical and structural properties can help us understand these processes, which in turn would help fabricate films having the desired characteristics [12]. The metal thin films deposited on nonmetal surfaces have attracted significant attention due to their potential applications [13]. The thin film surfaces exhibit complex structures, which are not adequately characterized by conventional methods. The investigation of thin film morphology with variation in thickness can give an insight about the growth mechanism of films, which is important for theoretical understanding [14]. The study of surface morphology evolution is also important for fabricating nanostructured materials in a controlled way to obtain desired properties. It is important to understand the kinetic growth mechanisms of thin films and thereby its dependence of the observed morphology on the parameters which govern the deposition process [13–17]. The growing surfaces are expected to develop self-affine or self-similar structure. The interface width can be described by the dynamic scaling method. The self-similar surfaces play important role in surface fabrication [18]. Several authors [18–22] have made efforts to understand the growth mechanism and surface roughening of growing thin film surface.

A self-similar system can be characterized by measures such as fractal dimension and multifractal spectra.

---

R. P. Yadav · A. K. Mittal  
Department of Physics, University of Allahabad,  
Allahabad 211002, UP, India

U. B. Singh  
Inter-University Accelerator Centre, Aruna Asaf Ali Marg,  
P. O. Box 10502, New Delhi 110 067, India

A. K. Mittal · S. Dwivedi (✉)  
K Banerjee Centre of Atmospheric and Ocean Studies,  
University of Allahabad, Allahabad 211002, UP, India  
e-mail: suneetdwivedi@gmail.com

Fractals and multifractals have been found useful for describing variety of structures found in nature and in basic sciences. A fractal is described by only one scaling exponent. The multifractal formalism generalizes this concept, which describes situations in which the scaling exponent depends on the position in the structure. The multifractal spectrum gives information about the fraction of sets whose measures scale with a particular scaling exponent [23]. It is found that the multifractal analysis of a thin film surface gives more detailed information of the surface as compared to fractal analysis. Due to easy implementation, high precision and low computation time, it has been used in various studies to characterize the evolution of surface morphology [23–31].

The atomic force microscopy (AFM) is an important technique to study the surface morphology of thin films [23]. The dependence of the surface morphology on the parameters of the deposition process can be revealed using the AFM technique. The analysis of the AFM images of thin film surface for different thickness can give insight about the evolution of surface morphology. It can also help in classifying different thin films growth mechanisms.

In this paper, we report the results of the multifractal analysis of the AFM images of gold thin films deposited by electron beam evaporation method at room temperature. The thin film surfaces of thickness of 20, 50 and 200 nm, respectively, were used for this purpose. The dependence of multifractal characteristics on thickness of films is studied. In Sect. 2, we briefly describe the experimental details. Section 3 explains the techniques used for the characterization of the gold thin film surface morphology. Results and discussions are given in Sect. 4. Conclusions are in Sect. 5.

## 2 Experimental details

The gold thin films of different thicknesses (20, 50 and 200 nm) were deposited on quartz substrates (of  $1 \times 1$  cm) by electron beam evaporation technique at room temperature and in a vacuum environment of  $\sim 10^{-6}$  Torr. The rate of deposition was 0.5 nm per sec. Before deposition, all the substrates were thoroughly cleaned. The thicknesses of the films were continuously monitored by quartz crystal monitor during deposition. The AFM is used to study the surface morphology of the pristine samples.

The surface morphology of the thin films was characterized under ambient condition using AFM images of size  $2.0 \times 2.0 \mu\text{m}$  and digitized into  $512 \times 512$  pixels. All the surface images were obtained in tapping mode with tip radius 20 nm.

## 3 Methods

### 3.1 Growth exponent

The two-dimensional root mean square (RMS) interface width  $\sigma$  of the AFM image with size  $M \times N$  pixels is given by:

$$\sigma = \sqrt{\frac{1}{MN} \sum_{i=0}^{M-1} \sum_{j=0}^{N-1} (z(i,j) - \langle z(i,j) \rangle)^2} \quad (1)$$

where  $z(i, j)$  denotes the surface height measured by the AFM at point  $(i, j)$ , and  $\langle z(i, j) \rangle$  represents the average given by.

$$\langle z(i,j) \rangle = \frac{1}{MN} \sum_{i=0}^{M-1} \sum_{j=0}^{N-1} z(i,j) \quad (2)$$

the average roughness is defined as follows

$$R_a = \frac{1}{MN} \sum_{i=0}^{M-1} \sum_{j=0}^{N-1} |z(i,j) - \langle z(i,j) \rangle| \quad (3)$$

the AFM image used here is quadrangular (with  $M = N = 512$  pixels). The thin films grown under non-equilibrium conditions are expected to be self-affine. It is general to observe power law scaling behaviour between interface width ( $\sigma$ ) and deposition time ( $t$ ). Since the deposition time is directly proportional to the film thickness ( $l$ ), therefore, the power law can be represented as [23].

$$\sigma(l) \propto l^\beta \quad (4)$$

where  $\beta$  is known as the growth exponent. The slope of  $\log \sigma$  versus  $\log l$  gives the value of  $\beta$ . The growth exponent  $\beta$  quantifies the increase in roughness with deposition time.

### 3.2 Multifractal characterization

We characterize the surfaces of the gold thin films using multifractal detrended fluctuation analysis (MFDFA), which may be considered as a special case of the more general multifractal formalism. Let the number of boxes of size  $\varepsilon$  covering the given structure (surface) is given as  $N(\varepsilon)$ , and the probability of the  $i$ th box is measured as  $p_i$ . Then, the partition function is defined by

$$Z(q, \varepsilon) = \sum_{i=1}^{N(\varepsilon)} (p_i)^q \quad (5)$$

for large positive (negative) values of  $q$ , the contributions from boxes having larger (smaller) measures dominate. In this way, different values of  $q$  probe the structure of the multifractal measure at different densities. Large positive

(negative) values of  $q$  probe very dense (rarefied) regions. The basic assumption of the multifractal formalism is that in the limit  $\varepsilon$  tending to 0,

$$p_i \sim \varepsilon^\alpha \tag{6}$$

where the scaling exponent  $\alpha$  can vary from box to box. Further, the number of boxes having scaling exponent between  $\alpha$  and  $\alpha + d\alpha$  is  $\sim \varepsilon^{-f(\alpha)}d\alpha$ ; here,  $f(\alpha)$  is a continuous function of  $\alpha$ . Hence, with these assumptions, the partition function (5) becomes,

$$Z(q, \varepsilon) = \int \varepsilon^{-f(\alpha)} \varepsilon^{2q} d\alpha \tag{7}$$

as  $\varepsilon$  tends to 0, this integral is dominated by the value  $\alpha_m$  of  $\alpha$  for which  $\alpha q - f(\alpha)$  has the smallest value. This value satisfies

$$\frac{d}{d\alpha} \{ \alpha q - f(\alpha) \}_{\alpha_m} = 0 \tag{8}$$

giving

$$f'(\alpha_m) = q \tag{9}$$

and

$$Z(q, \varepsilon) \sim \varepsilon^{\tau(q)} \tag{10}$$

where

$$\tau(q) = \alpha_m q - f(\alpha_m) \tag{11}$$

we have,

$$\frac{d\tau}{dq} = \alpha_m + \frac{d\alpha_m}{dq} q - f'(\alpha_m) \frac{d\alpha_m}{dq} = \alpha_m \tag{12}$$

where the last equality makes use of Eq. (8). Then, Eq. (10) yields

$$f(\alpha_m) = q \frac{d\tau}{dq} - \tau \tag{13}$$

as the value of  $q$  is varied from  $-\infty$  to  $\infty$ , the points  $[\alpha_m, f(\alpha_m)]$  trace a continuous curve called the multifractal spectrum. This spectrum is difficult to obtain directly from the definitions of  $\alpha$  and  $f(\alpha)$  but is easily obtained from the function  $\tau(q)$  using Eqs. (12) and (13). The function  $\tau(q)$  describes the scaling of the partition function, which is easily computed both for theoretical models and experimental data.

### 3.3 Multifractal detrended fluctuation analysis (MFDFA)

The one-dimensional multifractal detrended fluctuation analysis was developed for investigating the non-stationary time series. Suppose a time series is denoted by an array  $X(i), i = 1, 2, \dots, N$ . This series is

partitioned into segments of equal length  $n$  so that the total number of segments is  $N_n \equiv \text{int} [N/n]$ , the number of segments  $N_n$  clearly scales inversely with the segment length  $n$ . The segments are denoted by  $X_k, k = 1, 2, \dots, N_n$ . The value of the time series at the  $i$ th point of the segment  $X_k$ , denoted by  $X_k(i)$ , will be equal to  $X((k - 1)n + i)$ . The cumulative sum over each of the segments  $X_k$  is given by

$$C_k(i) = \sum_{j=1}^i X_k(j) \tag{14}$$

the trend of the cumulative sum is postulated to be a polynomial  $\tilde{C}_k(i)$  of some specified order. The coefficients of the polynomial are obtained by the method of least squares. The RMS fluctuation from the trend denoted by  $F(n, k)$  is given by

$$F^2(n, k) = \frac{1}{n} \sum_{i=1}^n \{ C_k(i) - \tilde{C}_k(i) \}^2 \tag{15}$$

in MFDFA, the function  $F(n, k)$  is taken to be the measure (of the  $k$ th segment of size  $n$ ), which is subjected to multifractal analysis. Now averaging over all segments, we obtained the  $q$ th-order fluctuation function defined by

$$F_q(n) \equiv \left\{ \frac{1}{N_n} \sum_{k=1}^{N_n} [F(n, k)]^q \right\}^{1/q} \tag{16}$$

where  $q$  can take any real value. The scaling behaviour of the fluctuation functions is obtained from the graphs of  $\log F_q(n)$  versus  $\log n$  for different  $q$  values. The slopes of the straight lines fitted over the linear portions of the graphs are denoted by  $h(q)$ . We, therefore, have

$$F_q(n) \sim n^{h(q)} \tag{17}$$

where  $h(q)$  are called the generalized Hurst exponents. The generalized Hurst exponents  $h(q)$  are related to the mass exponents  $\tau(q)$ , which describe the scaling of the partition function,

$$Z_q(n) \equiv \sum_{k=1}^{N_n} |F(n, k)|^q \sim n^{\tau(q)} \tag{18}$$

from Eqs. (16) and (17),

$$\begin{aligned} Z_q(n) &\equiv \sum_{k=1}^{N_n} |F(n, k)|^q \\ &= N_n \{ F_q(n) \}^q \sim n^{-D} (n^{h(q)})^q \sim n^{q h(q) - D} \end{aligned} \tag{19}$$

where,  $D$  is the dimension which determines the scaling of  $N_n$  with  $n$ .

Comparing Eqs. (18) and (19), we get

$$\tau(q) = q h(q) - D \tag{20}$$

the local roughness exponent or singularity strength  $\alpha$  and the singularity spectrum  $f(\alpha)$  are then obtained using Eqs. (12) and (13).

In case of 2D MF DFA [23–25], which is applied to characterize the 2D surface denoted by the 2D array  $X(i, j)$  with  $i = 1, 2, 3 \dots M$  and  $j = 1, 2, 3 \dots N$ , the overall fluctuation function for the surface is given by

$$F_q(n) = \left\{ \frac{1}{M_n N_n} \sum_{k_1=1}^{M_n} \sum_{k_2=1}^{N_n} [F(k_1, k_2, n)]^q \right\}^{1/q} \quad (21)$$

where the disjoint segments in the 1D case are replaced by disjoint squares of equal size  $n \times n$  for the 2D case.

### 3.4 Statistical test for multifractal analysis

The statistical significance of the observed multifractality is tested using the approach given by the Jiang and Zhou [32, 33]. The original surface data are shuffled to remove the sequential correlation. The same multifractal analysis is carried out for the shuffled data as for the original data. The two characteristic quantities defined as  $F = [f(\alpha_{\min}) + f(\alpha_{\max})]/2$  and  $\Delta\alpha = \alpha_{\max} - \alpha_{\min}$  are calculated for each singularity spectrum, and parametric values are compared with average values of shuffled surface data. To test the presence of multifractality, we impose a strict null hypothesis to investigate whether the singularity spectrum is wider than those produce by chance. Here,  $p$  value is computed for probability that the null hypothesis is true. Smaller  $p$  value gives the stronger evidence against the null hypothesis and tells that the presence of multifractality is statistically significant. The associated probabilities  $p_1$  and  $p_2$  of false alarm for multifractality are given as follows:

$$p_1 = \frac{\sum_n \theta[\Delta\alpha \leq \Delta\alpha_{shft}]}{n} \quad (22)$$

$$p_2 = \frac{\sum_n \theta[F \geq F_{shft}]}{n} \quad (23)$$

here,  $\theta$  is Heaviside step function and  $n$  is the total number of shuffling. The parameter  $\Delta\alpha_{shft}$  is the multifractal spectrum width of the shuffled surface, and  $F_{shft}$  is the  $F$  value of shuffled surface. The multifractal analysis approach is treated as significant, and the null hypothesis is rejected, if and only if  $p_1$  and  $p_2 \leq 0.01$ .

## 4 Results and discussion

The AFM micrographs of gold (Au) thin films of thickness 20, 50 and 200 nm deposited on quartz substrates are shown in Fig. 1. The increase in the grain size with

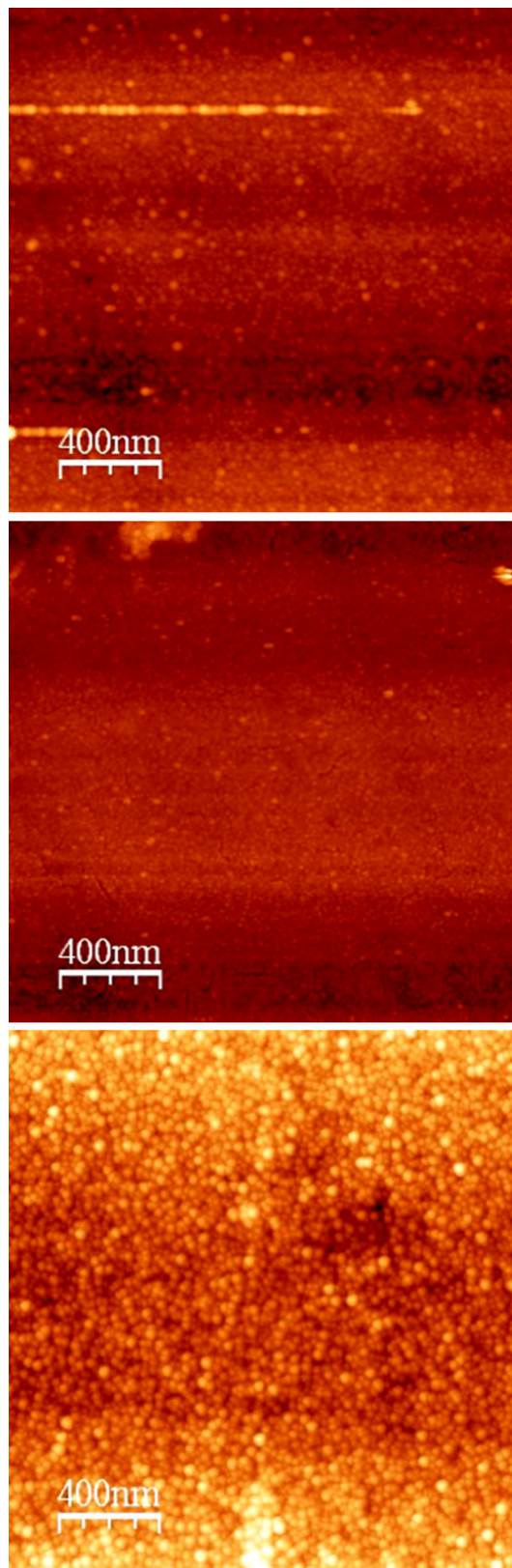


**Fig. 1** AFM images of the gold thin films at 20 nm (upper panel), 50 nm (middle panel) and 200 nm (lower panel)



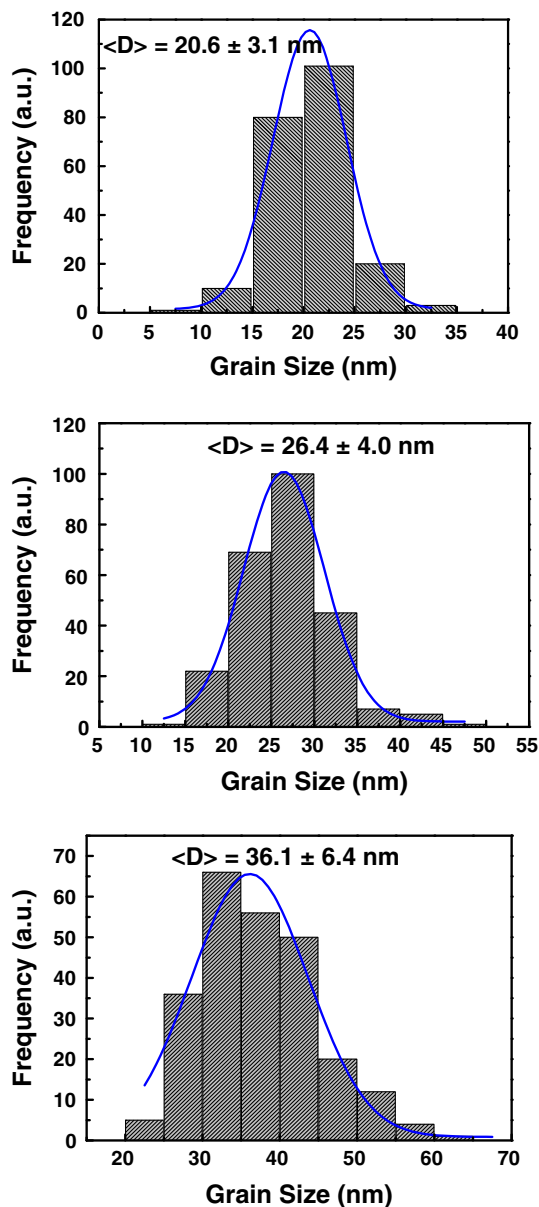


Fig. 2 Estimation of grain size of gold thin films

increase in the thickness of the Au films is evident from Fig. 1. The frequency distribution of the grain size is shown in Fig. 2. The grain size of Au films of thickness 20, 50 and 200 nm is  $20.6 \pm 3.1$ ,  $26.4 \pm 4.0$  and  $36.1 \pm 6.4$  nm, respectively. A similar behaviour has also been observed in [23] for LiF films in the thickness range of 10–40 nm, deposited by thermal evaporation and analysed by the AFM.

The interface width values ( $\sigma$  and  $R_a$ ) are determined for different thickness by using the method described in Sect. 3.1. The roughness values are shown in Table 1. Surface morphology is strongly affected by the aggregation, structure and grain size [12, 18, 23]. The average roughness

Table 1 Film thickness  $l$ , average roughness  $R_a$ , interface width  $\sigma$  and multifractal singularity spectrum for different thicknesses

$l$ (nm)	$R_a$ (nm)	$\sigma$ (nm)	$\alpha_{\max}$	$\alpha_{\min}$	$\Delta\alpha$	$f(\alpha_{\min})$	$f(\alpha_{\max})$	$\Delta f$
20	2.26	2.79	2.07	1.98	0.08	1.93	1.86	0.07
50	2.82	3.40	2.06	1.93	0.13	1.76	1.86	-0.10
200	4.48	5.48	2.12	1.96	0.16	1.91	1.66	0.26

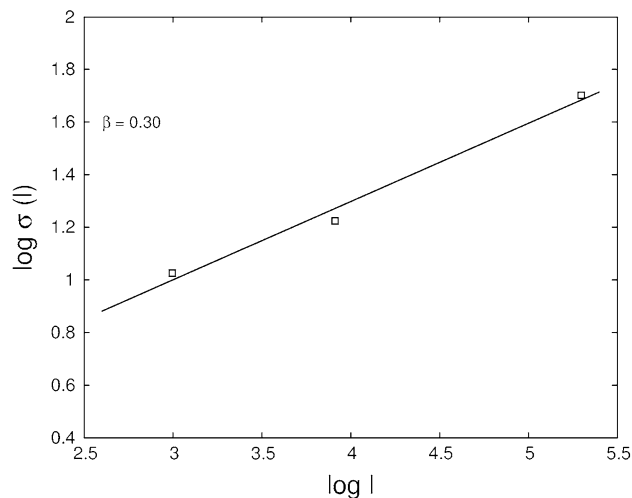
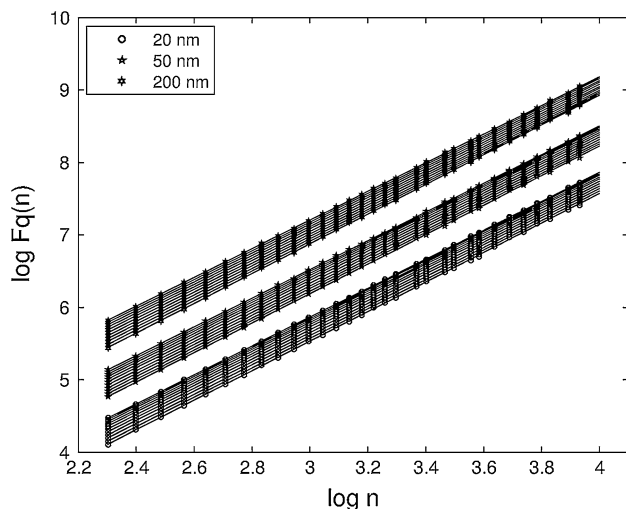


Fig. 3 Log–log plot of interface width versus film thickness. The slope of the best-fit straight line gives growth exponent ( $\beta$ )

( $R_a$ ) and interface width ( $\sigma$ ) increase with increasing thickness. However, these roughness parameters do not provide a complete description of the thin film surfaces. Local characteristics, traits and details about the shape of peaks and valleys are not revealed by these parameters. It is also found that the roughness parameters based on conventional theories depend on the sampling interval of the particular measuring instrument [23].

The evolution of surface morphology exhibits the growth process and microstructure of the thin film. It is also characterized by the dynamic scaling behaviour of the interface width. Figure 3 shows the evolution of thin films interface width ( $\sigma$ ) as a function of films thickness ( $l$ ). The growth exponent  $\beta$  (slope of the best-fit line in Fig. 3) is estimated to be 0.30 for the gold thin films. This value is close to those reported for Ag/Si at 300 K ( $\beta = 0.26$ ) [34], Fe/Si(111) at 323 K ( $\beta = 0.25$ – $0.32$ ) [35], Cu/Cu(1 0 0) at 160 K ( $\beta = 0.26$ ) [36], Au/Si(100) at room temperature ( $\beta = 0.37$ ) [37], Ag thin films on quartz substrate at room temperature ( $\beta = 0.29$ ) [38], Au/Si(111) prepared by radiofrequency sputtering at room temperature and anneal to 873 K ( $\beta = 0.38$ ) [17], Au/SiO<sub>2</sub> prepared by radiofrequency sputtering at room temperature ( $\beta = 0.30$ ) [13] and



**Fig. 4** Log  $F_q(n)$  versus log  $n$  for the thin films of thicknesses 20, 50 and 200 nm for different  $q$  values. The *solid lines* are the least squares fits to the data. The plots for 50 and 200 nm are shifted upward by 0.45 and 0.7 for clarity

SiO<sub>2</sub> thin films grown by plasma-enhanced chemical vapour deposition ( $\beta = 0.28$ ) [21]. The value of the growth exponent obtained is not very reliable because it is based on only three data points. However, the three points on the graph are consistent with the expected growth of interface width with thickness. Though unreliable, the value obtained is credible when compared with the values of growth exponent reported by other investigators.

We have performed multifractal detrended fluctuation analysis (MFDFA) on the AFM images using the method described in the Sect. 3.3. Figure 4 exhibits the dependence of the detrended fluctuations  $F_q(n)$  with respect to window scale  $n$  for different values of  $q$  to each thickness. The figure shows that for each  $q$  value, there is a power law scaling between  $F_q(n)$  and  $n$ . The slope of the straight lines obtained by least square regression of  $\log F_q(n)$  against  $\log n$  gives the scaling exponent value  $h(q)$ , which is a nonlinear decreasing function of  $q$  for each thickness as shown in Fig. 5. We computed the mass exponent  $\tau(q)$  for the different values of  $q$  using Eq. (20), which is also a nonlinear function of  $q$  suggesting that the surfaces under investigation have a multifractal nature. Thus, nonlinearity of scaling exponent  $h(q)$  and mass exponent  $\tau(q)$  is hallmark of presence of multifractal character in thin film surface. Here, it is important to note that the estimation of  $F_q(n)$  becomes statistically less significant for the greater values of  $q$  due to small size data. As a matter of fact, for larger values of  $|q| > 5$ , it is not possible to get clear power law scaling behaviour. In other words, the scale invariance behaviour is destroyed beyond  $|q| > 5$ . The difference in nonlinearity for these thin films surfaces can be clearly seen from Fig. 5. The deviation from linearity is greatest

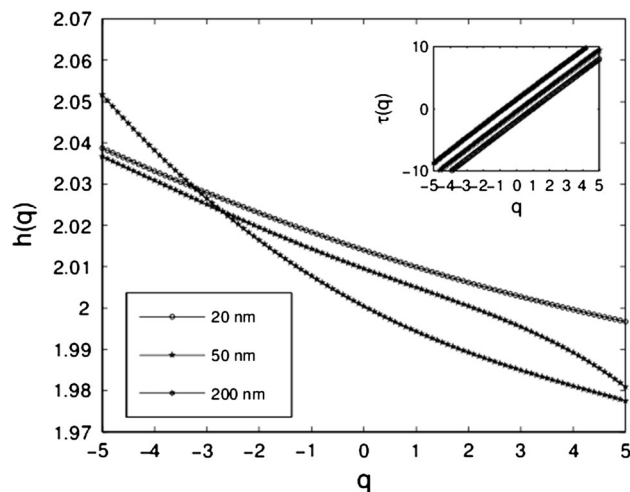


**Fig. 5** Scaling exponent  $h(q)$  as a function of  $q$ . The *inset* shows the mass exponent function  $\tau(q)$

for the thin film with thickness 200 nm; therefore, it is roughest amongst all the thin films surfaces.

Figure 6 shows the multifractal spectra obtained by using Eqs. (12) and (13). The multifractal spectrum parameters are summarized in Table 1. Figure 6 exhibits that  $f(\alpha)$  are continuous functions of  $\alpha$  and strongly depend on the film thickness. The shape and width of  $f(\alpha)$  spectrum are different for each thickness. We see that the shape of the multifractal spectra is hook-like to the left for 20 and 200 nm, while for 50 nm hook-like to the right [25]. It is found that with increase of thickness, the singularity spectrum becomes wider. Similar results were reported in the other studies [23, 39] of thin films surface morphology with different thickness. It means the surfaces with higher thicknesses are more irregular and surface becomes more complex and singular. The maximum and minimum singularities  $\alpha_{\max}$  and  $\alpha_{\min}$  are the singularity strengths associated with the region of sets, where the measures are the most and least singular, respectively [23, 25, 39]. The  $f(\alpha_{\max})$  and  $f(\alpha_{\min})$  values reveal the fractal dimension of two regions, which are characterized by their corresponding singularities  $\alpha_{\max}$  and  $\alpha_{\min}$ . Table 1 gives an idea about the list of the key parameters of the multifractal spectra of thin films with different thickness. From the table, we can see that the minimum singularity  $\alpha_{\min}$  decreases with thickness, while maximum singularity  $\alpha_{\max}$  increases. The multifractal spectrum width  $\Delta\alpha = \alpha_{\max} - \alpha_{\min}$  represents the range of the height distribution of probabilities. It is found that the probability distribution range is narrower for the surfaces with smaller interface width. The greater  $\Delta\alpha$  is associated with stronger multifractality, while the smaller  $\Delta\alpha$  is associated with weaker multifractality. It is also clear from Table 1 that the value of  $\Delta\alpha$  increases as the film thickness increases; therefore, the film becomes irregular and rougher with thickness.

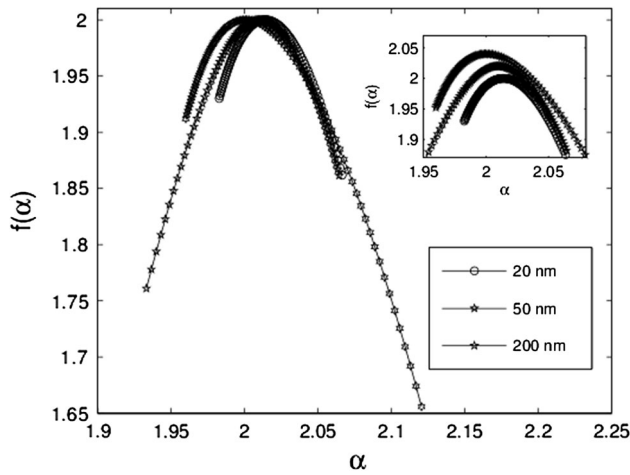


**Fig. 6** Multifractal spectra ( $f(\alpha)$  vs.  $\alpha$ ) of the gold thin film surfaces at different thickness. The inset picture gives the same information, but with curves for 50 and 200 nm shifted upwards by 0.02 and 0.04, respectively, for clarity

In multifractal formalism,  $\alpha_{\min}$  is associated with the maximum probability measure by  $P_{\max} \sim \varepsilon^{\alpha_{\min}}$ , where  $\varepsilon$  represents the scale approaching zero and is small quantity, whereas  $\alpha_{\max}$  is associated with minimum probability measure given by  $P_{\min} \sim \varepsilon^{\alpha_{\max}}$ . The spectral width  $\Delta\alpha$  can be used to describe the range of growth probability measure [23, 25, 39]. Here,  $f(\alpha_{\max})$  indicates the number of least growth probability with  $N_{P_{\min}} = N_{\alpha_{\max}} \sim \varepsilon^{-f(\alpha_{\max})}$  and  $f(\alpha_{\min})$  described the number of maximum probability such as  $N_{P_{\max}} = N_{\alpha_{\min}} \sim \varepsilon^{-f(\alpha_{\min})}$ . Thus, the difference of fractal dimension  $\Delta f = f(\alpha_{\min}) - f(\alpha_{\max})$  describes the height interval of multifractal spectrum. It also describes the ratio between the regions, where the distribution is most concentrated and most rarefied [25] which may be represented as follows

$$N_{P_{\max}}/N_{P_{\min}} \sim \varepsilon^{-\Delta f}$$

here  $\Delta f < 0$  means, there are more concentrated regions than rarefied site, where as  $\Delta f > 0$  means the contrary.

One may be concerned about the influence on the results due to the partitioning procedure leaving out some data points near the end. A look at Fig 4 shows that the  $\log F_q(n)$  versus  $\log n$  straight line fits are very good. If the boundary influence was very significant, the deviation of points from the straight lines would have been significantly larger, because different values of segment size  $n$  would leave out different amounts of data near the boundary. So we can conclude that the boundary influence is not significant.

To test the statistical significance of the extracted multifractality, each surface morphology data were shuffled 1,000 times to construct the surrogate surfaces. The surrogate surfaces were also analysed using the same

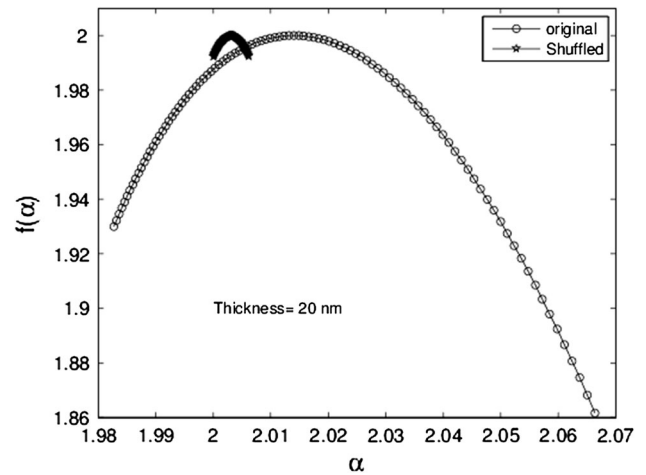


**Fig. 7** Multifractal spectra ( $f(\alpha)$  vs.  $\alpha$ ) of gold thin film surface of thickness 20 nm and its corresponding shuffled surface

technique. For 20-nm thin film, the multifractal spectra for the original surface and for a shuffled are shown in Fig. 7. The deviation of the multifractal spectra of the original surface data  $f(\alpha)$  and that of the shuffled surface data  $f_{shft}(\alpha_{shft})$  is clear from the figure. Out of the 1,000 shuffled surfaces, not even one had  $\Delta\alpha_{shft}$  more than the observed  $\Delta\alpha$  for the analysed thin film. Moreover, it is found that  $\Delta\alpha > \langle \Delta\alpha_{shft} \rangle$  and  $F < \langle F_{shft} \rangle$  for the gold thin film surface data. The associated probabilities of false alarm  $p_1$  and  $p_2$  are computed using Eqs. (22) and (23), respectively. It is found that the value of  $p_1$  and  $p_2$  is absolutely zero. Hence, the gold thin films under investigation are multifractal in nature.

### 5 Conclusion

In this study, we analysed the changes of surface morphology and scaling behaviour of gold thin films prepared by electron beam evaporation method on the quartz substrate for different thicknesses. The AFM was used to study the surface morphology, and conventional parameters such as interface width and average roughness were used to characterize these films. The multifractal analysis demonstrates that the film surfaces have multifractal nature. The parameters of multifractal spectra are used to characterize the growth and interface width of thin films. The multifractal analysis is shown to provide greater information in comparison with conventional methods. The statistical significance test confirms the multifractal character of the gold thin film surface morphology.

**Acknowledgments** RPY is thankful to the CSIR-UGC for providing financial support in the form of senior research fellowship.

## References

1. S. Link, M.A. El-Sayed, Spectral properties and relaxation dynamics of surface plasmon electronic oscillations in gold and silver nanodots and nanorods. *J. Phys. Chem. B* **103**, 8410–8426 (1999)
2. E.M. Fernandez, J.M. Soler, I.L. Garzon, L.C. Balbas, Trends in the structure and bonding of noble metal clusters. *Phys. Rev. B* **70**, 165403 (2004)
3. D.M. Kolb, Electrochemical surface science. *Angew. Chem. Int. Edn.* **40**, 1162–1181 (2001)
4. A. Dawson, P.V. Kamat, Semiconductor-metal nanocomposites photoinduced fusion and photocatalysis of gold-capped TiO<sub>2</sub> (TiO<sub>2</sub>/Gold) nanoparticles. *J. Phys. Chem. B* **105**, 960–966 (2001)
5. K. Kneipp, Y. Wang, H. Kneipp, L.T. Perelman, I. Itzkan, R. Dasari, M.S. Feld, Single molecule detection using surface-enhanced raman scattering (SERS) *phys. Rev. Lett.* **78**, 1667–1670 (1997)
6. X. Yu, Z.Q. Wang, Y.G. Jiang, F. Shi, X. Zhang, Reversible pH-Responsive surface: from superhydrophobicity to superhydrophilicity. *Adv. Mater.* **17**, 1289–1293 (2005)
7. M. Haruta, Size- and support-dependency in the catalysis of gold. *Catal. Today* **36**, 153–166 (1997)
8. J.F. Hainfeld, F.A. Dilmanian, D.N. Slatkin, H.M. Smilowitz, Radiotherapy enhancement with gold nanoparticles. *J. Pharm. Pharmacol.* **60**, 977–985 (2008)
9. C.A. Mirkin, R.L. Letsinger, R.C. Mucic, J.J. Storhoff, ADNA-based method for rationally assembling nanoparticles into macroscopic materials. *Nature* **382**, 607–609 (1996)
10. M. Bechelany, P. Brodard, J. Elias, A. Brioude, J. Michler, L. Philippe, Simple synthetic route for SERS-active gold nanoparticles substrate with controlled shape and organization. *Langmuir* **26**, 14364–14371 (2010)
11. J. Elias, M. Gizowska, P. Brodard, R. Widmer, Y. Dehazan, T. Graule, J. Michler, L. Philippe, Electrodeposition of gold thin films with controlled morphologies and their applications in electrocatalysis and SERS. *Nanotechnology* **23**, 255705 (2012)
12. H. You, R.P. Chiarello, H.K. Kim, K.Q. Vandervoort, X-Ray reflectivity and scanning-tunneling-microscope study of kinetic roughening of sputter-deposited gold films during growth. *Phys. Rev. Lett.* **70**, 2900–2903 (1993)
13. F. Ruffino, M.G. Grimaldi, F. Giannazzo, F. Roccaforte, V. Raineri, Atomic force microscopy study of the kinetic roughening in nanostructured gold films on SiO<sub>2</sub>. *Nanoscale Res. Lett.* **4**, 262–268 (2009)
14. F. Ruffino, V. Torrisi, G. Marletta, M.G. Grimaldi, Atomic force microscopy investigation of the kinetic growth mechanisms of sputtered nanostructured Au film on mica: towards nanoscale morphology control. *Nanoscale Res. Lett.* **6**, 112 (2011)
15. F. Ruffino, A. Irrera, R. De Bastiani, M.G. Grimaldi, Room-temperature grain growth in sputtered nanoscale Pd thin films: dynamic scaling behavior on SiO<sub>2</sub>. *J. Appl. Phys.* **106**, 084309 (2009)
16. F. Ruffino, V. Torrisi, G. Marletta, M.G. Grimaldi, Kinetic growth mechanisms of sputter-deposited Au films on mica: from nanoclusters to nanostructured microclusters. *Appl. Phys. A* **100**, 7–13 (2010)
17. F. Ruffino, M.G. Grimaldi, Atomic force microscopy study of the growth mechanisms of nanostructured sputtered Au film on Si (111): evolution with film thickness and annealing time. *J. Appl. Phys.* **107**, 104321 (2010)
18. O. Akhavan, AFM spectral analysis of self-agglomerated metallic nanoparticles on silica thin films. *Curr. Nanosci.* **6**, 116–123 (2010)
19. T. Karabacak, Y.-P. Zhao, G.C. Wang, T.M. Lu, Growth-front roughening in amorphous silicon films by sputtering. *Phys. Rev. B* **64**, 085323 (2001)
20. M.E.R. Dotto, S.S. Camargo Jr, Scaling law analysis of paraffin thin films on different surfaces. *J. Appl. Phys.* **107**, 014911 (2010)
21. A.Y. Gil, J. Cotino, A.W. Pietrzykowska, A.R.G. Elipe, Scaling behavior and mechanism of formation of SiO<sub>2</sub> thin films grown by plasma-enhanced chemical vapor deposition. *Phys. Rev. B* **76**, 075314 (2007)
22. S. Yim, T.S. Jones, Anomalous scaling behavior and surface roughening in molecular thin-film deposition. *Phys. Rev. B* **73**, 161305(R) (2006)
23. R.P. Yadav, S. Dwivedi, A.K. Mittal, M. Kumar, A.C. Pandey, Fractal and multifractal analysis of LiF thin film surface. *Appl. Surf. Sci.* **261**, 547–553 (2012)
24. G.-F. Gu, W.-X. Zhou, Detrended fluctuation analysis for fractals and multifractals in higher dimensions. *Phys. Rev. E* **74**, 061104 (2006)
25. C. Liu, X.-L. Jiang, T. Liu, L. Zhao, W.-X. Zhou, K. Yuan, Multifractal analysis of the fracture surfaces of foamed polypropylene/polyethylene blends. *Appl. Surf. Sci.* **255**, 4239–4245 (2009)
26. J.W. Kantelhardt, S.A. Zschiegner, E. Koscielny-Bunde, S. Havlin, A. Bunde, H.E. Stanley, Multifractal detrended fluctuation analysis of nonstationary time series. *Phys. A* **316**, 87–114 (2002)
27. T.C. Halsey, M.H. Jensen, L.P. Kadanoff, I. Procaccia, B.I. Shraiman, Fractal measures and their singularities: the characterization of strange sets. *Phys. Rev. A* **33**, 1141–1151 (1986)
28. Z. Moktadir, M. Kraft, H. Wensink, Multifractal properties of pyrex and silicon surfaces blasted with sharp particles. *Phys. A* **387**, 2083–2090 (2008)
29. Z. Yu, L. Yee, Y.Z. Guo, Relationships of exponents in multifractal detrended fluctuation analysis and conventional multifractal analysis. *Chin. Phys. B* **20**, 090507 (2011)
30. X.Y. Qian, G.F. Gu, W.X. Zhou, Modified detrended fluctuation analysis based on empirical mode decomposition for the characterization of anti-persistent processes. *Phys. A* **390**, 4388–4395 (2011)
31. M.R. Niu, W.X. Zhou, Z.Y. Yan, Q.H. Guo, Q.F. Liang, F.C. Wang, Z.H. Yu, Multifractal detrended fluctuation analysis of combustion flames in four-burner impinging entrained-flow gasifier. *Chem. Eng. J.* **143**, 230–235 (2008)
32. Z.-Q. Jiang, W.-X. Zhou, Multifractality in stock indexes: fact or fiction? *Phys. A* **387**, 3605–3614 (2008)
33. Z.-Q. Jiang, W.-X. Zhou, Multifractal analysis of Chinese stock volatilities based on the partition function approach. *Phys. A* **387**, 4881–4888 (2008)
34. C. Thompson, G. Palasantzas, Y.P. Feng, S.K. Sinha, J. Krim, X-ray-reflectivity study of the growth kinetics of vapor-deposited silver films. *Phys. Rev. B* **49**, 4902 (1994)
35. J. Chevrier, V.L. Thanh, R. Buys, J. Derrien, A RHEED study of epitaxial growth of iron on a silicon surface: experimental evidence for kinetic roughening. *Europhys. Lett.* **16**, 737 (1991)
36. H.J. Ernst, F. Fabre, R. Folkerts, J. Lapujoulade, Observation of growth instability during low temperature molecular beam epitaxy. *Phys. Rev. Lett.* **72**, 112–115 (1994)
37. E. Rodriguez-Canas, J.A. Aznarez, A.I. Oliva, J.L. Sacedon, Relationship between the surface morphology and the height distribution curve in thermal evaporated Au thin films. *Surf. Sci.* **600**, 3110–3120 (2006)
38. G. Palasantzas, J. Krim, Scanning tunneling microscopy study of the thick film limit of kinetic roughening. *Phys. Rev. Lett.* **73**, 3564–3567 (1994)
39. W. Wang, A. Li, X. Zhang, Y. Yin, Multifractality analysis of crack images from indirect thermal drying of thin-film dewatered sludge. *Phys. A* **390**, 2678–2685 (2011)